Sensitivity Analysis of Microstrip Tree S-Parameters by Using Tensorial Analysis of Networks

Lucius Ramifidisoa, Rivo Randriatsiferana, Sébastien Lalléchère, Zhifei Xu, Blaise Ravelo

Progress In Electromagnetics Research B, Vol. 87, 193–209, 2020

Sensitivity Analysis of Microstrip Tree *S*-Parameters by Using Tensorial Analysis of Networks

Lucius Ramifidisoa[1], Rivo Randriatsiferana[2, *], Sébastien Lalléchère[3], Zhifei Xu[4], and Blaise Ravelo[5]

Abstract—This paper introduces a tensorial analysis of networks (TAN) applied to a tree asymmetrical structure. To illustrate the TAN concept easily, the present investigation is applied to a three-port structure represented by a Y-tree topology. The unfamiliar method of TAN circuit modelling is elaborated from the graph topology. The fast formulation of the Y-matrix model of the structure is established from branch and mesh space TAN analyses. The TAN model is validated with commercial tool simulation and measurements from DC up to 0.5 GHz in the frequency domain and two different waveform signals in the time domain. The proof of concept circuit is implemented in microstrip technology on an FR4-epoxy dielectric substrate. Mapping sensitivity analysis with respect to the Y-tree RLC-parameters is realized by showing that local variations around initial set of R, L, and C do not equally influence reflection and transmission coefficients over the frequency bandwidth. If a similar impact is observed at the lowest frequency, maximum variations up to 250% show the importance of parameters ranking to improve both microstrip design and modelling.

1. INTRODUCTION

Nowadays, the tradition of electronic circuit design engineering undeniably incorporates the dependence of numerical approaches which use different mathematical methods as transmission-line matrix (TLM) [1], method of moments (MoM) [2], finite element method (FEM) [3], nodal method basically used to develop SPICE netlists [4], and artificial neural network (ANN) method [5]. These numerical solvers are integrated in the computer aided design (CAD) simulators which become popular success as standard commercial tools for the electromagnetic (EM) simulations of printed circuit boards (PCBs) [6–10]. These CADs are usually employed to predict the undesirable effects as electromagnetic interference (EMI), electromagnetic compatibility (EMC), and signal integrity (SI) issues [11–13] susceptible to degrading the performance of modern PCBs. The electrical interconnects constitute one of the undesirable effects notably for high-density PCBs [14, 15].

Relevant prediction and direction were suggested for the PCB SI and power integrity (PI) design engineering [16, 17]. The influence of electrical interconnects on PCB performances must be investigated during the design phase [14, 15]. Emphatically, constant progress is necessary for the modelling of multi-port electronic components [18, 19]. However, the existing commercial tools [6–10] dedicated to the electrical interconnect effects may be time-consuming on pre- and post-processing in addition to the computation time. The Z- and Y-matrix analytical parameters are the most useful and efficient

Received 14 April 2020, Accepted 29 July 2020, Scheduled 18 August 2020

* Corresponding author: Rivo Randriatsiferana (rivo.randriatsiferana@univ-reunion.fr).

[1] ENSET, University of Antsiranana, Antsiranana, Madagascar. [2] University of La Reunion, LE2P Lab, Saint Denis, Reunion, France. [3] Université Clermont Auvergne (UCA), CNRS, SIGMA Clermont, Institut Pascal, Aubière, France. [4] EMC Laboratory, Missouri University of Science and Technology, Rolla, MO 65401, USA. [5] Nanjing University of Information and Science Technology, Nanjing, Jiangsu 210044, China.

expressions for designing and characterizing electronic and microwave devices [20–23]. The frequency-dependent Z- and Y-matrix modellings enable to predict the performances of microelectronic packaged circuits [23]. Different analytical methods have been proposed to extract equivalent immittance matrices of electrical interconnect networks [14, 24–26]. The interconnect modellings are mostly established based on transmission line (TL) approaches [25–28]. One of the most efficient way to elaborate the multi-port interconnect model with immittance matrices can be performed with graph theory.

The proposed research work aims to introduce an alternative fast computational method to determine multi-port network equivalent immittance matrix with a particular graph theory. The unfamiliar analytical method under study is developed based on the Tensorial Analysis of Networks (TAN) [29–33]. In brief, the TAN was initiated by Kron in 1930s for the electrical machine modelling [29]. Several decades later, the Kron's method was exploited by Maurice and his team for solving EMC issues of the complex electrical and electronic systems [30–32]. More recently, the TAN method was also used for the S-matrix modelling of multiport structures as PCB interconnections [32] and coupled coaxial cables [33]. Compared to the existing research work on the TAN method available in the literature [34–37], the present paper claims the following differences:

- The simplicity and improvement of TAN methodology implementation for multi-port structure with, in the present paper, the possibility to calculate directly all the S-matrix elements in the overall frequency band in one-pass via the direct consideration of multi-port interconnect Y-matrix,
- The analytical and verification methodology of the sensitivity analyses with the vectorial approach,
- And then, in terms of R, L, and C approximated element consideration via the integration of the Hammerstad-Jensen [38, 39].

The present paper is organized in three main sections. Section 2 is focused on the theoretical investigation of asymmetric microstrip Y-tree implemented based on Hammerstad-Jensen model [38, 39]. The methodology explaining how to use the TAN method for quick cash extraction of frequency-dependent Y-matrix is established. Then, the S-matrix model is calculated from Y-to-S matrix transform [40]. Section 3 discusses the unfamiliar TAN method with consideration of microstrip Y-tree proof of concept (POC). In addition, sensitivity analysis (SA) is introduced for evaluating the dominant parameters on the Y-tree S-parameter variations. Then, the last section is the conclusion.

2. THEORETICAL INVESTIGATION ON THE TAN COMPUTATIONS

The present section develops the theoretical approach on the TAN modelling of applied to three-port networks represented by a Y-tree topology.

2.1. Topological Description

To determine the equivalent S-parameters, the three access ports of the circuit are excited by voltage sources at its each terminal port $M_{1,2,3}$. As illustrated in Fig. 1, the voltage sources are denoted $U_{1,2,3}$. Fig. 1(a) represents the distributed structure under study. This interconnect network is supposed constituted by three different microstrip TLs $\mathrm{TL}_{k=1,2,3}$ (interconnecting nodes M_k and the middle node M_0) with characteristic impedance Z_k and physical length d_k. The equivalent circuit composed of RLC-elements is shown in Fig. 1(b).

The black box representing the Y-tree is proposed in the diagram of three-port system shown in Fig. 2. The circuit is assumed as excited by voltage source U_k at each node M_k. From this system view, based on the access each branch electrical parameters, we can denote the symbolic port voltage and current written as, respectively:

$$[U(s)] = [\ U_1(s) \quad U_2(s) \quad U_3(s)\ ] \tag{1}$$

$$[I(s)] = \begin{bmatrix} I^1(s) \\ I^2(s) \\ I^3(s) \end{bmatrix} \tag{2}$$

by denoting the Laplace variable $s = j\omega$ with $j^2 = 1$ and the angular frequency ω. Each branch of the tree is assumed as an equivalent T-cell as shown in Fig. 3 by neglecting the resistive loss. It is built with identical series impedance and parallel admittance expressed in the following paragraphs.

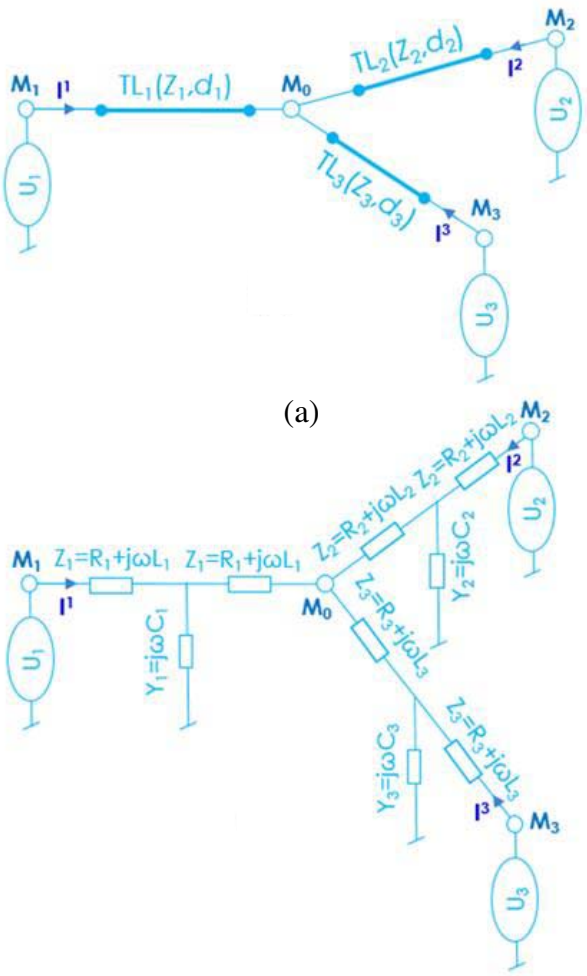

Figure 1. (a) Distributed and (b) lumped element equivalent network of the Y-tree circuit under study.

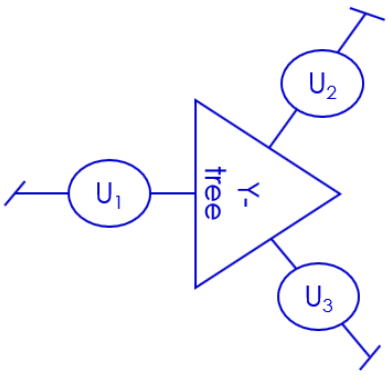

Figure 2. Black box representation of Y-tree introduced in Fig. 1.

The equivalent lumped circuit of the Y-tree is established with Hammerstad-Jensen model [38, 39]. Each branch tree is constituted by T-cells built with:

$$Z_k(s) = R_k + L_k s \tag{3}$$

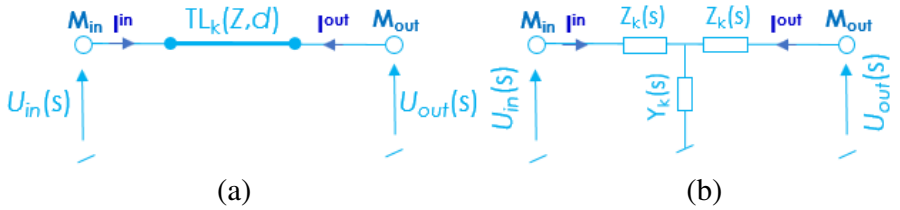

Figure 3. LC equivalent lumped circuit of an elementary TL.

series impedance and:

$$Y_k(s) = C_k s \tag{4}$$

parallel admittance is shown in Fig. 1(b). According to the circuit theory, with a, $b = 1, 2, 3$, the equivalent Y-matrix:

$$[Y] = Y^{ab} \tag{5}$$

is analytically defined by the relationship:

$$[I(s)] = [Y(s)] \times [U(s)] \tag{6}$$

where the structure excitation voltage source is given in Equation (1).

2.2. Analytical Modelling

For the interconnect modelling, the TAN method can be implemented in the five phases as described in the following paragraphs.

2.2.1. Phase 1: Graph Description and Topological Parametrization

The TAN modelling can be started with the elaboration of the Kron's branch allowing to represent both the branch and mesh space variables of the problem. Fig. 4 depicts the Kron's graph equivalent to the circuit shown in Fig. 1(b).

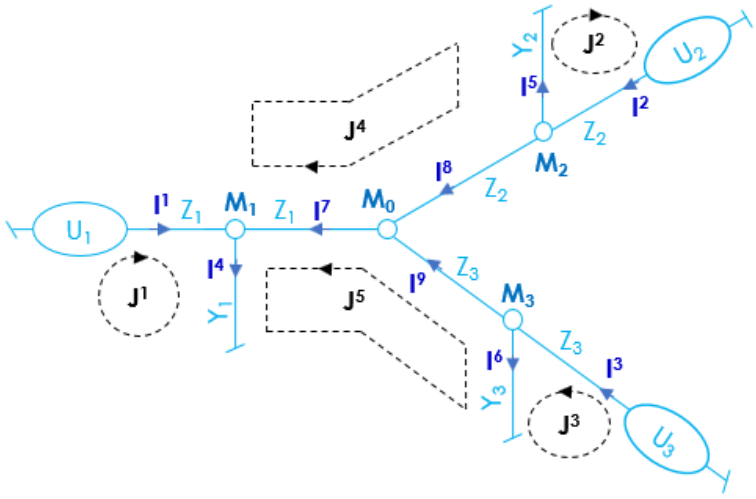

Figure 4. Kron's graph equivalent to the circuit introduced in Fig. 1(b).

The topological analysis of the graph enables the topological parameters addressed in Table 1.

Table 1. Topological parameters.

Parameter number	Branch	Node	Mesh	Port
Value	$B = 9$	$N = 5$	$M = 5$	$P = 3$

2.2.2. Phase 2: Branch Space Analysis

In the branch space, the problem can be formulated by the covariable voltage:

$$V_b(s) = [\ V_1(s) \quad ... \quad V_B(s)\ ] \tag{7}$$

the contravariable current:

$$I^b(s) = \begin{bmatrix} I^1(s) \\ \vdots \\ I^B(s) \end{bmatrix} \tag{8}$$

and the double covariable branch impedance:

$$Z_{bb}(s) = \begin{bmatrix} Z_{11}(s) & 0 & \cdots & 0 \\ 0 & Z_{22}(s) & \ddots & \vdots \\ \vdots & \ddots & \ddots & 0 \\ 0 & \cdots & 0 & Z_{BB}(s) \end{bmatrix} \tag{9}$$

$(b = 1, 2, ..., B)$ whose extra-diagonal elements are null. With subscripts $b = 1, ..., 9$ the Z_{bb} diagonal elements can be rewritten as:

$$\begin{cases} Z_{bb=\{1,2,3\}}(s) = Z_b(s) \\ Z_{bb=\{4,5,6\}}(s) = \dfrac{1}{Y_{b-3}(s)} \\ Z_{bb=\{7,8,9\}}(s) = Z_{b-6}(s) \end{cases}. \tag{10}$$

2.2.3. Phase 3: Mesh Space Analysis

First, the branch to mesh connectivity of graph shown in Fig. 4 is written as:

$$C_b^m = \begin{bmatrix} U_{33} & O_2^3 \\ U_{33} & \begin{bmatrix} 1_2 \\ -U_{22} \end{bmatrix} \\ O_{33} & \begin{bmatrix} 1_2 \\ -U_{22} \end{bmatrix} \end{bmatrix} \tag{11}$$

with:

$$U_{22} = \begin{bmatrix} 1 & 0 \\ 0 & 1 \end{bmatrix} \tag{12}$$

and:

$$U_{33} = \begin{bmatrix} 1 & 0 & 0 \\ 0 & 1 & 0 \\ 0 & 0 & 1 \end{bmatrix} \tag{13}$$

are two- and three-dimension identity matrices;

$$O_2^3 = \begin{bmatrix} 0 & 0 \\ 0 & 0 \\ 0 & 0 \end{bmatrix} \tag{14}$$

is a two column and three row zero matrix;

$$O_{33} = \begin{bmatrix} 0 & 0 & 0 \\ 0 & 0 & 0 \\ 0 & 0 & 0 \end{bmatrix} \tag{15}$$

is a zero three-dimension square matrix, and

$$1_2 = \begin{bmatrix} 1 & 1 \end{bmatrix} \tag{16}$$

is a 1-D unity matrix. In the mesh space, with m, $n = 1, 2, ..., M$, the covariable voltage, contravariable current, and double covariable impedance are linked to the branch space variables by the Einstein notation, respectively:

$$\Lambda_m = C_m^b V_b \tag{17}$$

$$J^n = C_b^n I^b \tag{18}$$

$$\Omega_{mn} = C_m^b Z_{bb} C_n^b. \tag{19}$$

We recall that based on the tensorial notation, $C_m^b = C_n^b$ is the transpose of $C_b^m = C_b^n$.

2.2.4. Phase 4: Y-Matrix Model Extraction

From previously established mesh voltage, current, and impedance, the metric equation written in Einstein notation is yielded:

$$\Lambda_m = \Omega_{mn} J^n. \tag{20}$$

By identification with the relationship earlier written in Eq. (3), the Y-tree Y-matrix can be extracted algebraically from Equation (20) knowing that:

$$\begin{cases} I^{1,2,3} = J^{1,2,3} \\ U^{1,2,3} = \Lambda^{1,2,3} \end{cases} \tag{21}$$

By explicit relationship in Eq. (20) with subtensors defined by subscripts $\alpha, \mu = 1, 2, ..., P$ and $\beta, \nu = P+1, ..., M$, we have:

$$\begin{bmatrix} U_\mu \\ O_\nu \end{bmatrix} = \begin{bmatrix} \Omega_{\mu\alpha} & \Omega_{\mu\beta} \\ \Omega_{\nu\alpha} & \Omega_{\nu\beta} \end{bmatrix} \begin{bmatrix} J^\alpha \\ J^\beta \end{bmatrix} \tag{22}$$

with:

$$O_\nu = \begin{bmatrix} 0 \\ \vdots \\ 0 \end{bmatrix} \tag{23}$$

being the zero $M - P$ size 1-rank tensor. Substituting the solution of the 2nd line of Eq. (22) into the first line, we have the Y-matrix:

$$[Y] = \left\{ \Omega_{\mu\alpha} - \Omega_{\mu\beta} (\Omega_{\nu\beta})^{-1} \Omega_{\nu\alpha} \right\}^{-1}. \tag{24}$$

2.2.5. Phase 5: S-Matrix Model Extraction

In difference to the immittances, the S-matrix must be computed with consideration of source and load reference impedances. Therefore, an appropriated transform relationship is needed to determine the S-matrix from Y- or Z-matrices. For the considered Y-structure, it is more convenient to proceed with Y-matrix. Therefore, the S-matrix model of the Y-tree can be determined from previous Equation (24) with the Y-to-S matrix transform [36]. Accordingly, the S-matrix can be extracted from the matrix relation:

$$[S(s)] = \{U_{33} - R_0 [Y(s)]\} \times \{U_{33} + R_0 [Y(s)]\}^{-1} \tag{25}$$

with R_0 being the S-parameters reference impedance.

2.3. Methodological Pedagogy

Compared to most of classical electrical and electronic engineering modelling methods, the TAN approach remains unfamiliar to most of PCB or electronic circuit design engineers. To overcome this limitation, it is important to describe a simple methodology enabling to practice the TAN formalism. In brief, the different phase of circuit TAN modelling introduced in the previous subsection can be reorganized in seven successive steps. Fig. 5 addresses the actions associated with the different steps from the starting to ending points. The different steps consist mainly of the actions:

- Physical and geometrical parameter definitions;
- RLC electrical parameter definitions and access ports identification;
- Topological parameter (branch, node, network, mesh, port) definitions;
- The TAN graph must be drawn with disjoint meshes;
- Analytical calculations of branch variables ($[V_b]$, $[I^b]$, $[Z_{bb}]$) and mesh variables ($[U_m]$, $[J^n]$, $[Z_{mn}]$);
- And impedance size reduction with the internal mesh impedance element elimination via mesh sub-matrix identification.

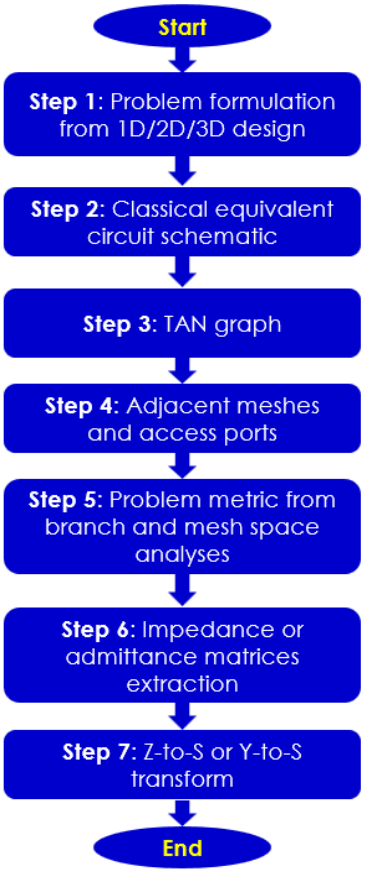

Figure 5. Workflow of TAN modelling for electrical and electronic circuits.

2.4. Recall on Microstrip TL Theory

To verify the relevance of this circuit theory, validation results of Y-tree with SA are proposed in the next section. However, it would be important to recall the basic equations of microstrip TL theory.

2.4.1. Considered Model of Microstrip Line for Determining RLC Lumped Network

Each constituting TL of the considered tree circuit is implemented as microstrip line. Fig. 6 represents the 3-D design of the microstrip structure including the geometrical parameters. The physical parameters are the width and length denoted as w and d. The substrate is characterized by the dielectric material with thickness h and relative permittivity ε_r.

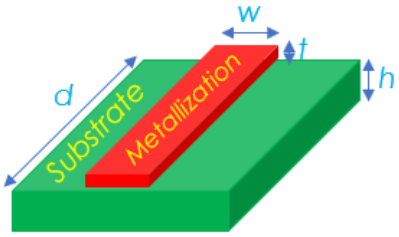

Figure 6. Microstrip structure and its geometrical parameters.

The equivalent lumped circuit of the Y-tree is established with Hammerstad-Jensen model [17, 18]. By denoting:

$$x = \frac{w}{h}, \tag{26}$$

the effective permittivity and characteristic impedance can be estimated as, respectively:

$$\varepsilon_{eff} \approx 0.5\left\{\varepsilon_r + 1 + (\varepsilon_r - 1)\left[0.04(1-x)^2 + \frac{1}{\sqrt{1+12/x}}\right]\right\} \tag{27}$$

$$Z_c \approx \frac{Z_{air}}{2\pi\sqrt{\varepsilon_{eff}}} \ln\left(\frac{5.98h}{w+t}\right). \tag{28}$$

By denoting the vacuum absolute permittivity ε_0 and permeability μ_0, we have:

$$Z_{air} = \sqrt{\frac{\mu_0}{\varepsilon_0}}. \tag{29}$$

The wave speed, wavelength, and phase constant of the line are denoted respectively as:

$$v = \frac{c}{\sqrt{\varepsilon_{eff}}} \tag{30}$$

$$\beta(\omega) = \frac{2\pi}{\lambda(\omega)} \tag{31}$$

with c being the vacuum light speed. Knowing that the wavelength is defined by:

$$\lambda(\omega) = \frac{2\pi v}{\omega} \tag{32}$$

the phase constant of Eq. (31) becomes:

$$\beta(\omega) = \frac{\omega\sqrt{\varepsilon_{eff}}}{c}. \tag{33}$$

This recall that microstrip line theory enables to determine the LC model of Y-tree introduced in the following paragraph.

2.4.2. LC Model of Single Microstrip Line

The L and C lumped parameters are assumed constant and independent of the frequency. By denoting σ as the conductor metal conductivity of microstrip line depicted in Fig. 6, the analytical equations in

function microstrip physical parameters are expressed as:

$$R = \frac{d}{\sigma w t} \tag{34}$$

$$L = \frac{Z_{air} c \ln\left(\dfrac{5.98h}{w+t}\right)}{2\pi\varepsilon_{eff} d} \tag{35}$$

$$C = \frac{2\pi\varepsilon_{eff} d}{Z_{air} c \ln\left(\dfrac{5.98h}{w+t}\right)}. \tag{36}$$

3. VALIDATION RESULTS

The present section discusses the previously developed S-matrix modelling applied to a Y-tree proof-of-concept (POC). Comparisons between modelled and simulated results are discussed.

3.1. Description of the Proof of Concept

A microstrip tree circuit was designed as the proof of concept of the developed TAN model. The following paragraphs describe the structure and its equivalent lumped circuit.

3.1.1. Design Circuit

To validate the developed TAN model, we have considered the 3-D design of Y-tree circuit POC shown in Fig. 7. The three access ports are fed by voltage sources $U_k = \{1, 2, 3\}$, and TL branches are defined

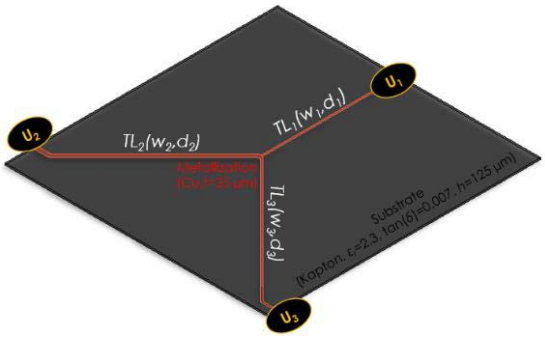

(a)

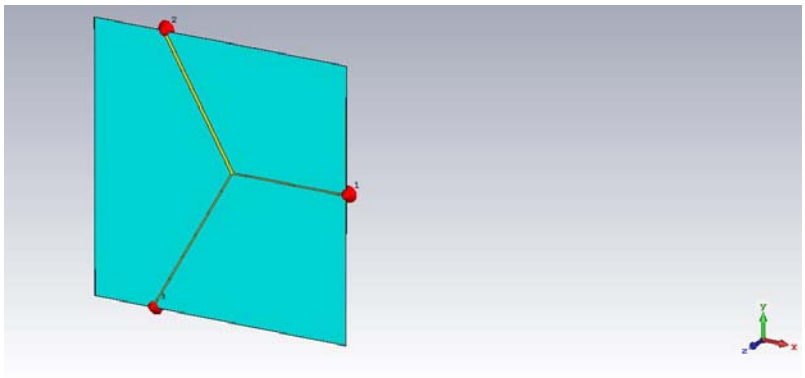

(b)

Figure 7. (a) ADS® and (b) CST® 3-D design of Y-tree POC.

by their physical width w_k and length d_k. This interconnect circuit is designed with two different EM solvers of commercial tools:

- in the Momentum® environment of ADS® RF and microwave circuit simulator from Keysight Technologies® for Fig. 7(a),
- and in CST MWS® environment for Fig. 7(b).

We emphasize that this POC circuit is implemented in microstrip technology printed on a Kapton dielectric substrate with Copper based metallization as illustrated earlier in Fig. 6. The physical parameters of these constituting materials constituting the POC circuit are indicated in Table 2. To realize the computations, the physical and electrical parameters constituting TL elements of the tree are listed in Table 3. The electrical parameters R_k, L_k, and C_k with $k = \{1, 2, 3\}$ are calculated from physical ones by using Equations (34) and (35).

Table 2. Proof-of-concept circuit constituting material parameters.

Components	Description	Parameter	Value
Dielectric substrate	Material	Kapton	-
	Relative permittivity	ε_r	2.3
	Loss tangent	$\tan(\delta)$	0.007
	Thickness	h	125 µm
Metallization	Material	Copper (Cu)	-
	Thickness	t	355 µm
	Conductivity	σ	58 MS/m

Table 3. Y-tree physical and electrical parameters.

TL	**Geometrical and electrical parameters**		
	Length	Width	RLC parameters
TL_1	$d_1 = 50\,\text{mm}$	$w_1 = 0.6\,\text{mm}$	$R_1 \approx 43\,\text{m}\Omega$
			$L_1 \approx 4.25\,\text{nH}$
			$C_1 \approx 9\,\text{pF}$
TL_2	$d_2 = 60\,\text{mm}$	$w_2 = 1.43\,\text{mm}$	$R_2 \approx 22\,\text{m}\Omega$
			$L_2 \approx 2.55\,\text{nH}$
			$C_2 \approx 2.28\,\text{pF}$
TL_3	$d_3 = 70\,\text{mm}$	$w_3 = 0.6\,\text{mm}$	$R_3 \approx 59\,\text{m}\Omega$
			$L_3 \approx 11.9\,\text{nH}$
			$C_3 \approx 12.66\,\text{pF}$

3.2. Discussion on Calculated and Simulated Results

After Matlab programming of previous TAN model, comparisons between calculation ("Calc.") and simulation with ADS® and CST® results from 0 to 0.5 GHz are elaborated in the present subsection.

3.2.1. Frequency Domain Results

As aforementioned, the frequency domain analysis is based on S-parameters from Equation (23) following the workflow introduced earlier in Fig. 5 and ADS® simulations. Therefore, Figs. 8 and 9

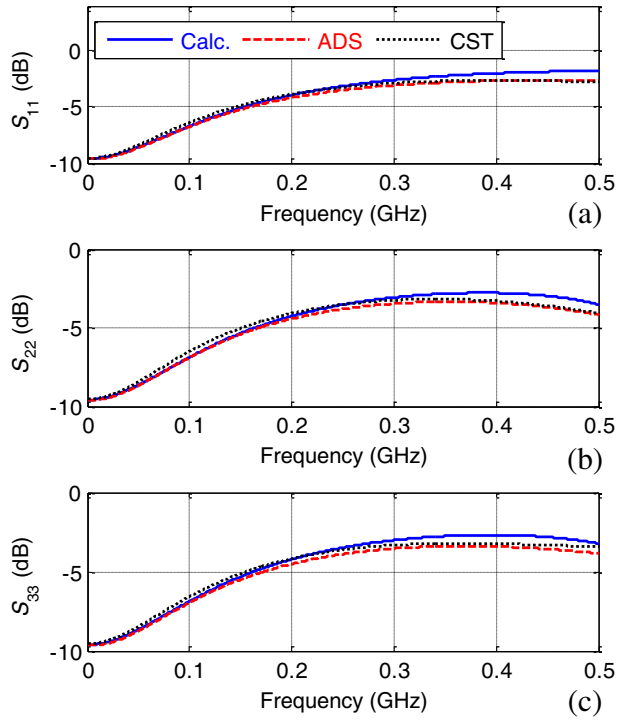

Figure 8. Calculated and simulated magnitudes: (a) S_{11}, (b) S_{22} and (c) S_{33}.

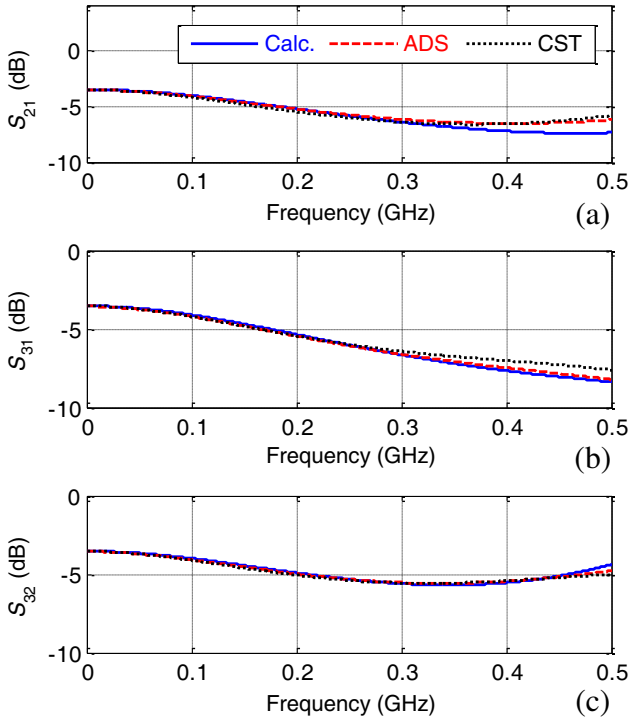

Figure 9. Calculated and simulated magnitudes: (a) S_{21}, (b) S_{31} and (c) S_{32}.

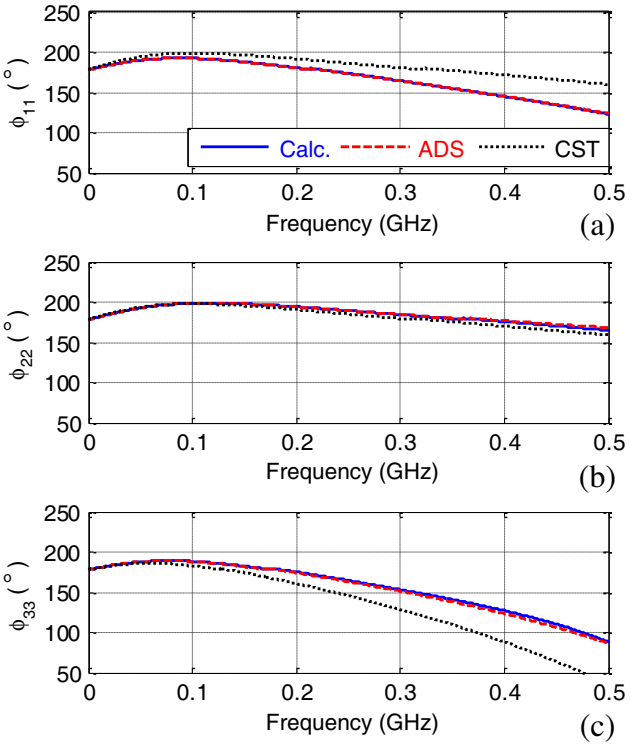

Figure 10. Calculated and simulated phases: (a) S_{11}, (b) S_{22} and (c) S_{33}.

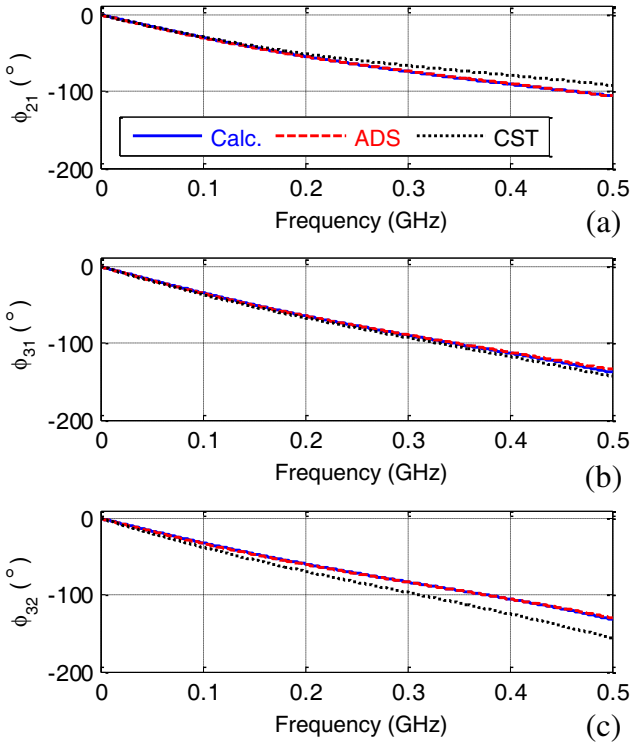

Figure 11. Calculated and simulated phases: (a) S_{21}, (b) S_{31} and (c) S_{32}.

display the magnitudes of Y-tree proof-of-concept reflection and transmission coefficients, respectively in function of frequency f:

$$|S_{k,l}|_{\mathrm{dB}} = 20\log|S_{k,l}(jf)|\,, \tag{37}$$

and the associated phases are shown in Figs. 10 and 11 which are defined by:

$$\varphi_{k,l} = \arg\left[S_{k,l}(jf)\right] \tag{38}$$

with integers $k, l = \{1, 2, 3\}$. For the magnitude and phase comparative results, the calculated S-parameters from TAN model are in good agreement with ADS® and CST® simulations. The slight discrepancies between the calculated and simulated S-parameter magnitudes and also the phase shifts, above 0.3 MHz, are mainly due to the following imperfections:

- The skin depth effect, at higher frequencies, which are not included in the approximated values of R, L, and C elements from the TL interconnect elements,
- The inaccuracies of the full wave structure meshing sizes which are hardly matched to wide frequency bands.

3.2.2. Time Domain Results

In addition to previous validation, time domain analyses in function of time variable t were performed by comparing the transient responses from the TAN model and simulations. To do this, we considered two different input signals:

- Bi-exponential waveform:

$$v_{In}(t) = \exp\left(\frac{-t}{\tau_1}\right) - \exp\left(\frac{-t}{\tau_2}\right). \tag{39}$$

  with $\tau_1 = 2\tau_2 = 2\,\mathrm{ns}$,
- and an arbitrary waveform signal.

During the analysis, the transient computations were performed up to $t_{\max} = 16\,\mathrm{ns}$. As a consequence, we obtain the results plotted in Figs. 12(a) and 12(b) through output port_1 and port_2, respectively by injecting v_{In} at port_1. The time domain results with arbitrary waveform input are given in Fig. 13. Despite the slight ringing of simulated results, the calculated time domain ones present a good prediction of the output signal behaviour for both cases of considered inputs.

3.3. SA Mapping with Kron's Formulation

The Kron's methodology was successful for a variety of applications, e.g., complex networks modelling [30, 31] and PCB SI analyses [31]. The SA can be used by means of mathematical formulations regarding the microwave design equations, regarding the number, diversity, and nature of inputs (components, tracks, impedances) subject to intrinsic variations. In this context, SA, jointly with the analytical formulation extracted from Kron's procedure, is of utmost importance to highlight most influential parameters. Different objectives may be expected from SA, e.g., how input variations of a given mapping (from experiments, numerical model, mathematical formulation, etc.) affect the variability of its output parameters. Whereas a large diversity of techniques is available when considering SA at global stage (so called global sensitivity analysis, GSA, when considering inputs over a large interval), the problem is rather tricky at local stage (i.e., local sensitivity analysis, LSA, in the vicinity of a given set of inputs). Indeed, Saltelli et al. [41] have explained the difficulty to properly assess the adjoint sensitivity of the given output (through a precise computing of derivatives from each of the input parameters). Most of the studies in this framework focuse on GSA. Since LSA requires an accurate evaluation of the influence of small perturbations in the vicinity of input value:

$$\left[\hat{X}\right] = \begin{bmatrix} \hat{X}^1 \\ \vdots \\ \hat{X}^Q \end{bmatrix} \tag{40}$$

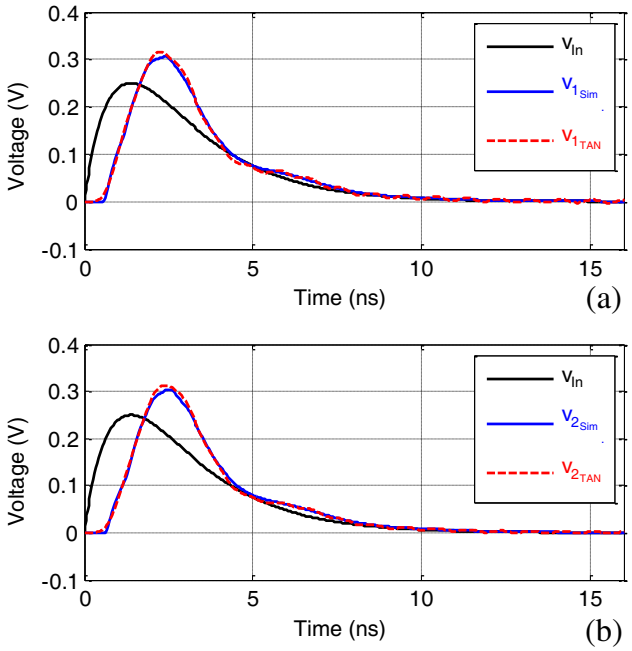

Figure 12. Calculated and simulated transient responses through output: (a) port$_1$ and (b) port$_2$ with bi-exponential input.

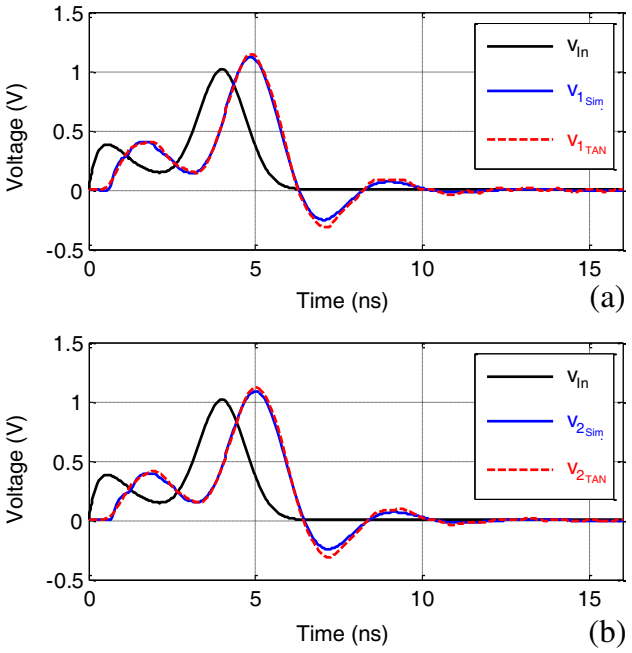

Figure 13. Calculated and simulated transient responses through output: (a) port$_1$ and (b) port$_2$ with arbitrary waveform input.

with the approximated values of vector $\hat{X}$ where Q stands for the number of input parameters, in function of the impacts to the S-matrix element output quantity:

$$\hat{S} = h(\hat{X}) \tag{41}$$

In this work, the mapping function $S(\cdot)$ may refer to one component (magnitude) of the S-matrix given in relation (14). The interest of TAN formalism is demonstrated in the following regarding the reflection coefficients $|S_{kk}|$ ($k = 1, 2, 3$) and the transmission ones $|S_{21}|$, $|S_{31}|$ and $|S_{32}|$, see Figs. 14–16. The corresponding input parameters are given as follows:

$$\begin{cases} X^1 = R_1 \\ X^2 = R_2 \\ X^3 = R_3 \\ X^4 = L_1 \\ X^5 = L_2 \\ X^6 = L_3 \\ X^7 = C_1 \\ X^8 = C_2 \\ X^9 = C_3 \end{cases} \tag{42}$$

where $Q = 9$. LSA is then derived in the vicinity of $\hat{X}$ through h-gradient as follows:

$$\nabla h|_{\hat{X}} = \left(..., \alpha^i|_{\hat{X}}, ...\right) \tag{43}$$

or

$$\nabla h|_{\hat{X}} = \left(..., \frac{\partial h}{\partial X^i}\bigg|_{\hat{X}}, ...\right) \tag{44}$$

The LSA methods mostly refer to the influence of each input, one-a-time by assessing coefficient in Equation (9) numerically or analytically [33]. The results given in Figs. 14–16 have to be compared

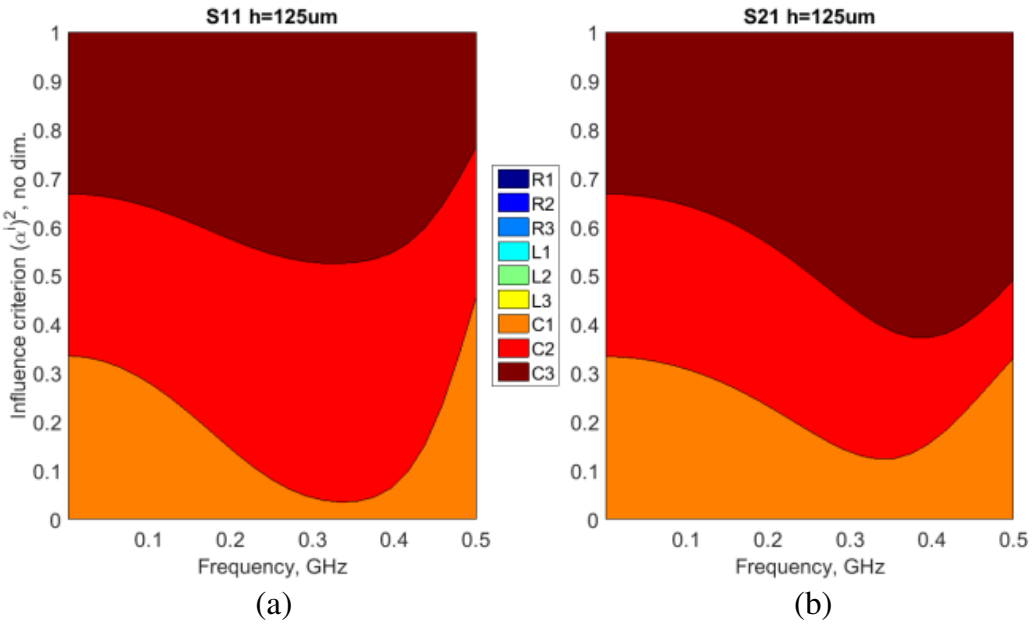

Figure 14. Influence of inputs (equivalent electrical parameters R_k, L_k, and C_k with $k = 1, 2, 3$) regarding: (a) S_{11} and (b) S_{21} coefficients.

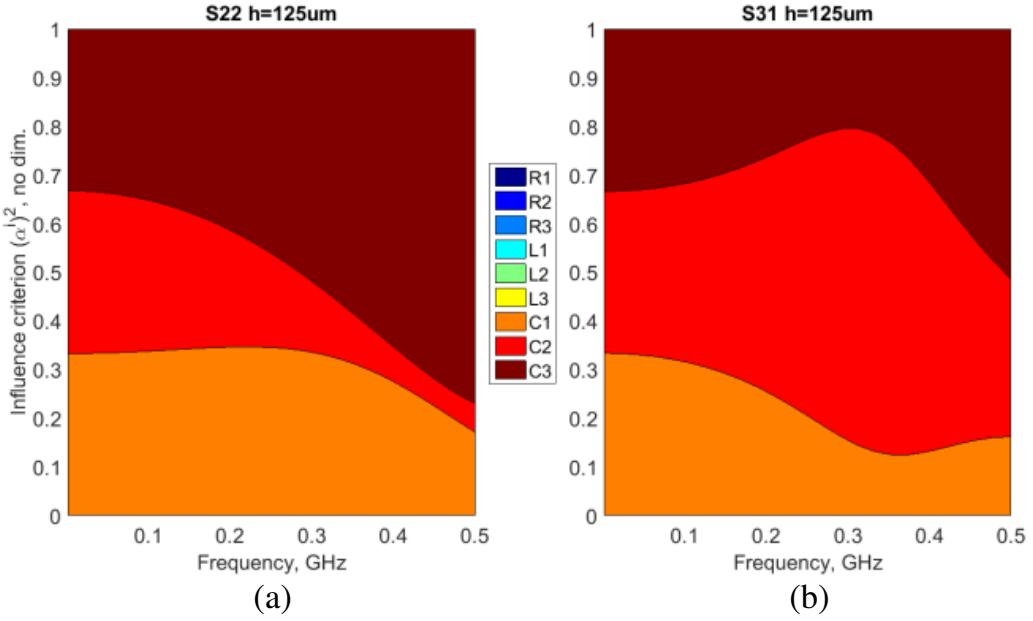

Figure 15. Influence of inputs (equivalent electrical parameters R_k, L_k, and C_k with $k = 1, 2, 3$) regarding: (a) S_{22} and (b) S_{31} coefficients.

to S-parameters simulations respectively in Figs. 8–11. By normalizing vector in relation (16) and computing normalized square of coefficients ($i = 1, ..., Q$), we define LSA components as given in Figs. 14–16. It is noticed that three parameters play major roles: C_k comparatively to R_k and L_k ($k = 1, 2, 3$) whereas the three main parameters C_k have similar impacts at low frequency bandwidth (below 100 MHz), and LSA allows the accurate assessment of most influential parameters at higher frequency. Thus, by considering Figs. 14–16 (left side), it is noted that the respective impact of C_k ($k = 1, 2, 3$) parameter is weaker from 0.2 to 0.4 GHz when considering S_{kk}-parameters. This influence

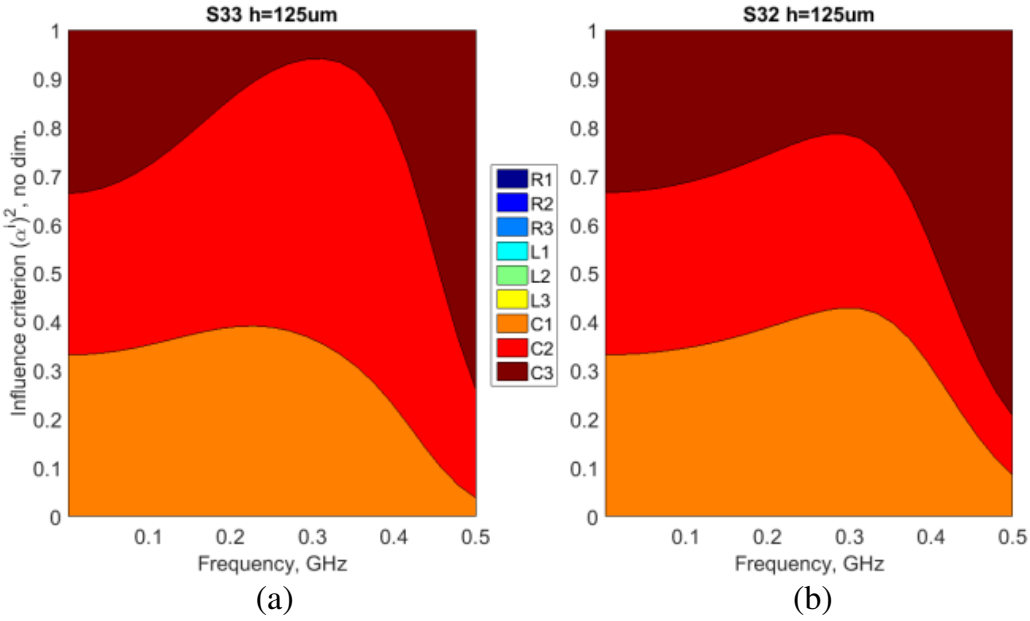

Figure 16. Influence of inputs (equivalent electrical parameters R_k, L_k, and C_k with $k = 1, 2, 3$) regarding: (a) S_{33} and (b) S_{32} coefficients.

increases at higher frequency (around 0.5 GHz), making C_k-value the most important one for S_{kk}. Due to the assumed geometrical input values (i.e., widths and lengths of tracks), it was expected that C_3-parameters would be of utmost importance. Indeed, it is the most influential parameter at higher frequency. The previous results have demonstrated the ability of Kron's method to provide analytical formulation of Y-tree microstrip modeling, enabling a precise evaluation of most influential parameters over the whole frequency bandwidth.

4. CONCLUSION

An efficient S-matrix modelling of multi-port interconnect networks is investigated. The developed model is aimed to solve electronic or electrical problems based on the unfamiliar TAN formalism. The methodology of TAN approach is described. It consists of successive computation steps from the graph representation to the immittance matrix expressions. The different steps are formulated with electrical tensorial variables with relationships written with compact Einstein notations. The final step of the TAN approach is the S-matrix extraction from the T-matrix calculated with the established problem metric.

The developed TAN model is validated with a POC of Y-tree interconnect PCB implemented in microstrip technology. The comparison between TAN calculations and simulations with two different commercial tools is discussed in both the frequency and time domains. As expected in theory, the calculated and simulated multi-port S-parameters from 0 to 0.5 GHz are in very good agreement. In addition, two different waveform signals are considered from time domain analyses. Once more, a good correlation between calculated and simulated time domain results is confirmed.

In addition to the modelling aspect, a particular study is reported on the SA analyses in function of the Y-tree parameters onto the S-parameters. As a result, the dominant TL parameters of the Y-tree structure are assessed via a particularly relevant SA.

ACKNOWLEDGMENT

This research work was supported in part by NSFC under Grant 61971230 and 61601233, and in part by Jiangsu Distinguished Professor program and Six Major Talents Summit of Jiangsu Province (2019-

DZXX-022), and in part by the Postgraduate Research & Practice Innovation Program of Jiangsu Province under Grant SJKY19_0974, and in part by the Priority Academic Program Development of Jiangsu Higher Education Institutions (PAPD) fund.

REFERENCES

1. Hoefer, W. J. R., "The transmission-line matrix method — Theory and applications," *IEEE Trans. MTT*, Vol. 33, No. 10, 882–893, Oct. 1985.
2. Ney, M., "Method of moments as applied to electromagnetic problems," *IEEE Trans. MTT*, Vol. 33, No. 10, 972–980, Oct. 1985.
3. Jin, J., *The Finite Element Method in Electromagnetics*, John Wiley & Sons, New York, USA, 1993.
4. Rizzoli, V., A. Costanzo, F. Mastri, and A. Neri, "A general SPICE model for arbitrary linear dispersive multiport components described by frequency-domain data," *Proc. 2003 IEEE MTT-S Int. Microwave Symp. Digest*, Vol. 1, 9–12, Philadelphia, PA, USA, Jun. 8–13, 2003.
5. Krishna, K. S. R., J. L. Narayana, and L. P. Reddy, "ANN models for microstrip line synthesis and analysis," *Int. J. Elect. Syst. Sci. Eng.*, Vol. 1, 196–200, 2008.
6. https://www.3ds.com/products-services/simulia/products/cst-studio-suite/, accessed 2019.
7. https://www.ansys.com/products/electronics/ansys-hfss, accessed 2019.
8. https://altairhyperworks.com/product/FEKO/Applications-Antenna-Design, accessed 2019.
9. https://www.keysight.com/us/en/assets/7018-02343/brochures/5990-4819.pdf, accessed 2019.
10. EM/EMC Simulation Software, https://www.emcos.com/?product-types=em-simulation-software, accessed 2019.
11. Schuster, C. and W. Fichtner, "Parasitic modes on printed circuit boards and their effects on EMC and signal integrity," *IEEE Trans. EMC*, Vol. 43, No. 4, 416–425, Nov. 2001.
12. Archambeault, R., C. Brench, and S. Connor, "Review of printed-circuit-board level EMI/EMC issues and tools," *IEEE Trans. EMC*, Vol. 52, No. 2, 455–461, May 2010.
13. Kim, J. and E. Li, "Special issue on PCB level signal integrity, power integrity, and EMC," *IEEE Trans. EMC*, Vol. 52, No. 2, 246–247, May 2010.
14. Ruehli, A. E. and A. C. Cangellaris, "Progress in the methodologies for the electrical modeling of interconnects and electronic packages," *Proceedings of the IEEE*, Vol. 89, No. 5, 740–771, 2001.
15. Ruan, A., J. Yang, L. Wan, B. Jie, and Z. Tian, "Insight into a generic interconnect resource model for Xilinx Virtex and Spartan series FPGAs," *IEEE Trans. CAS-II: Express Briefs*, Vol. 60, No. 11, 801–805, Nov. 2013.
16. Buckwalter, J. F., "Predicting microwave digital signal integrity," *IEEE Trans. Advanced Packaging*, Vol. 32, No. 2, 280–289, May 2009.
17. Jun, F., X. Ye, J. Kim, B. Archambeault, and A. Orlandi, "Signal integrity design for high-speed digital circuits: Progress and directions," *IEEE Trans. EMC*, Vol. 52, No. 2, 392–400, May 2010.
18. Ruehli, A. E. and A. C. Cangellaris, "Progress in the methodologies for the electrical modeling of interconnects and electronic packages," *Proc. of the IEEE*, Vol. 89, No. 5, 740–771, 2001.
19. Charlet, F. and J. F. Carpentier, "Extraction of 3D interconnect impedances using edge elements without gauge condition," *Proc. Int. Conf. on Simulation of Semiconductor Processes and Devices*, 143–146, Kobe, Japan, Sep. 4–6, 2002.
20. Chen, M., D. Shi, Y. Li, L. Zhu, and H. Liu, "Research on branches group based method for adding mutual inductance branches to Y-matrix and Z-matrix," *Proc. 2014 IEEE PES General Meeting Conference & Exposition*, 1–5, National Harbor, MD, USA, Jul. 27–31, 2014.
21. Wojnowski, M., M. Engl, and R. Weigel, "Considerations on impedance matrix determination for accurate passive device characterization," *Proc. 2007 IEEE Workshop SPI*, 117–120, Genova, Italy, May 13–16, 2007.

22. Tu, C., J. Bao, Y. Du, and W. Wu, "An improved design method for asymmetric RF MEMS tunable filter utilizing admittance matrix," *Proc. 2010 IEEE Int. Conf. on Microwave and Millimeter Wave Technology*, 1766–1769, Chengdu, China, May 8–11, 2010.
23. Chiariello, A. G., A. Girardi, C. Iorio, R. Izzi, T. Lessio, A. Maffucci, and S. Ventre, "Efficient evaluation of the frequency-dependent impedance matrix of full-package structures," *Proc. 2010 IEEE 14th Workshop on SPI*, 127–130, Hildesheim, Germany, May 9–12, 2010.
24. Ymeri, H., B. Nauwelaers, K. Maex, D. De Roest, S. Vandenberghe, and M. Stucchi, "Admittance matrix calculations of on-chip interconnects on lossy silicon substrate using multilayer Green's function," *Proc. 2001 IEEE Topical Meeting on Silicon Monolithic Integrated Circuits in RF Systems. Digest of Papers (IEEE Cat. No. 01EX496)*, 50–59, Ann Arbor, MI, USA, Sep. 14, 2001.
25. Sun, Y.-Y., "Immittance matrices of multiconductor transmission lines," *Journal of the Franklin Institute*, Vol. 307, No. 1, 59–67, Jan. 1979.
26. Xu, J. and Y.-H. Lv, "System-level construction of multiconductor transmission line inductance matrix," *Proc. 2009 3rd IEEE Int. Symp. on Microwave, Antenna, Propagation and EMC Technologies for Wireless Communications*, 903–906, Beijing, China, Oct. 27–29, 2009.
27. Hou, R. and C. Taibin, "Y parameter matrix and calculation method built for multi-port network based on graph theory," *Proc. 2011 IEEE 3rd International Conference on Communication Software and Networks*, 621–623, Xi'an, China, May 27–29, 2011.
28. Ravelo, B., "Behavioral model of symmetrical multi-level T-tree interconnects," *Progress In Electromagnetics Research B*, Vol. 41, 23–50, 2012.
29. Kron, G., *Tensor Analysis of Networks*, Wiley, New York; Chapman & Hall, London, 1939.
30. Maurice, O., A. Reineix, P. Hoffmann, B. Pecqueux, and P. Pouliguen, "A formalism to compute the electromagnetic compatibility of complex networks," *Advances in Applied Science Research*, Vol. 2, No. 5, 439–448, 2011.
31. Maurice, O., *Elements of Theory for Electromagnetic Compatibility and Systems*, Bookelis, Aix en Provence, France, 2017.
32. Ravelo, B. and O. Maurice, "Kron-Branin modeling of Y-Y-tree interconnects for the PCB signal integrity analysis," *IEEE Trans. on Electromagnetic Compatibility*, Vol. 59, No. 2, 411–419, Apr. 2017.
33. Cholachue, C., B. Ravelo, A. Simoens, and A. Fathallah, "Fast S-parameter TAN model of N-port lumped structures," *IEEE Access*, Vol. 7, No. 1, 72505–72517, Dec. 2019.
34. Xu, Z., Y. Liu, B. Ravelo, and O. Maurice, "Modified Kron's TAN modeling of 3D multilayer PCB," *Proc. of 11th International Workshop on Electromagnetic Compatibility of Integrated Circuits, EMC Compo 2017*, 242–247, St. Petersburg, Russia, Jul. 4–8, 2017.
35. Xu, Z., J. Fan, and O. Maurice, "Sensitivity analysis of PCB interconnect and package with TAN formalism," *Proc. of 2019 12th International Workshop on the Electromagnetic Compatibility of Integrated Circuits (EMC Compo)*, 81–83, Hangzhou, China, 2019.
36. Xu, Z., Y. Liu, B. Ravelo, and O. Maurice, "Multilayer power delivery network modeling with modified Kron's method (MKM)," *Proc. of 16th Int. Symposium on Electromagnetic Compatibility (EMC) Europe 2017*, 1–6, Angers, France, Sep. 4–8, 2017.
37. Xu, Z., Y. Liu, B. Ravelo, J. Gantet, N. Marier, and O. Maurice, "Direct time-domain TAN model of 3D multilayer hybrid PCB: Experimental validation," *IEEE Access*, Vol. 6, No. 1, 60645–60654, Dec. 2018.
38. Gupta, K. C., R. Garg, and I. Bahl, *Microstrip Lines and Slotlines*, Artech, Dedham, MA, 1979.
39. Hammerstad, E. and O. Jensen, "Accurate models for microstrip computer aided design," *Proc. 1980 IEEE MTT-S Int. Microwave Symp. Digest*, 407–409, Washington, DC, USA, May 28–30, 1980.
40. Frickey, D. A., "Conversions between $S, Z, Y, h, ABCD$, and T parameters which are valid for complex source and load impedances," *IEEE Trans. on MTT*, Vol. 42, No. 2, 205–211, Feb. 1994.
41. Saltelli, A., S. Tarantola, F. Campolongo, and M. Ratto, *Sensitivity Analysis in Practice: A Guide to Assessing Scientific Models*, John Wiley & Sons, 2004.